2010 IEEE/ASME International Conference on
Advanced Intelligent Mechatronics
Montréal, Canada, July 6-9, 2010

Position Sensorless BDCM Control with Repetitive Position-Dependent Load Torque

*Hung-Chi Chen (IEEE Member)
*Department of Electrical Engineering,
National Chiao Tung University, HsinChu, Taiwan.
hcchen@mail.nctu.edu.tw

*Chih-Kai Huang
Energy and Environment Laboratories,
Industrial Technology Research Institute, HsinChu, Taiwan.
Jeff.Huang@itri.org.tw

***Abstract*- This paper addresses the position sensorless control for brushless DC motor (BDCM) with repetitive position-dependent load torque which is a function of the absolute rotor position (not incremental rotor position). The robust sensorless control is composed of sensorless control and robust speed control. In order to commutate winding currents, the former one estimates the incremental rotor positions from the motor terminal voltages without any position sensor. In order to reduce the speed variations due to position-dependent load, a robust speed control is developed without estimating the absolute rotor position and other system parameter. In this paper, the effects of position-dependent load on the speed variations and the commutation intervals are studied in first. It shows that the position-dependent load can be estimated from the commutation intervals. Then, we develop the position sensorless control based on sensing terminal voltage from sensorless circuit and the robust speed control with adaptive gain. Finally, some simulated results have been given to demonstrate the robust performance of the proposed sensorless control for the position-dependent loads.**

I. INTRODUCTION

Compared to all the variable-speed motors like the induction motors (IMs), the synchronous reluctance motors (SRMs) and the brushless DC motors (BDCMs) [1], the latter two are free from the rotor exciting loss and rotor copper loss and, therefore, possess higher efficiency than the widely used induction motors (IMs). Moreover, because of the unusual power circuits for SRMs, BDCMs are gradually utilized as the high-efficiency compressor motors. In the normal operation of BDCMS, the rotor positions are sensed to commutate the winding current adequately. Unfortunately, in the refrigeration application, the high-temperature refrigerants will surround the compressor motor and the general position sensor such as Hall elements cannot be used. In order to operate BDCMs without any position sensors, developing sensorless control is important.

To solve it, many sensorless control methods had been proposed to replace the function of the position sensor. They can be divided into two groups according to the waveforms of the drawn motor currents: one group is discontinuous winding currents (or called square-wave currents) and the other is continuous currents (or called sinusoidal-wave currents). Since there always is a floating motor terminal in the former group, some schemes including sensing terminal voltages and diode currents are used to directly obtain the rotor positions [2-4]. However, it is noted that all the sensorless control methods obtain the incremental rotor positions, not absolute rotor positions.

In addition, there are several types of compressors in the market for various refrigeration systems and various cooling capacities. However, from the motor's point of view, the load torques of compressor motors are the functions of the absolute rotor position and thus, they are repetitive. Several load curves for popular domestic compressors are shown in Fig. 1. We can find that the torque curve is nearly constant for scroll compressors but there is a significantly peak torque in the single-piston rotary compressor. In fact, such extremely alternating torque would contribute to the compressor speed ripple and thus, introduce the noise and vibrations to the overall system [5]. That is, scroll compressors possess better performances than the single-piston rotary compressor.

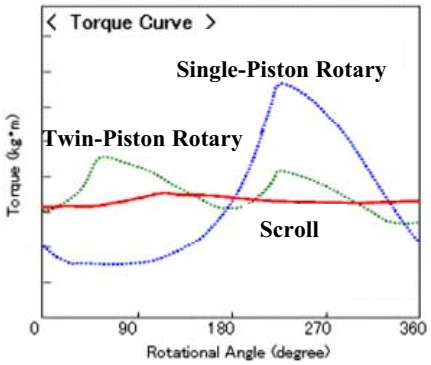

Fig. 1. Typical torque curves for various types of compressors.

However, it is noted that high performance (i.e. low torque ripple) often implies high production-cost. In order to promote variable-speed refrigeration systems to market with acceptable prices, the low-cost single-piston rotary compressors become the only one choice. Consequently, the single-piston rotary compressors using BDCMs are preferred in the high-efficiency and low-cost variable-speed refrigeration systems.

In order to less the effect of the position-dependent load on the overall system, the development of robust speed control becomes very important. Many control methods had been developed to deal with the nonlinear load torque including the position-dependent loads [6-8]. However, the above methods are complex and not working in the sensorless operation.

In this paper, a position sensorless control is proposed where the unknown repetitive position-dependent load torque is estimated, and then the varying gain is used to adjust the duty ratio simultaneously. The provided simulated results also demonstrate the proposed sensorless control.

II. Position-Dependent Load Torque

Due to the hermetic and high-temperature environment in refrigerant compressor, it is not easy to directly sense the actual motor position and rotating speed. On the other hand, entire refrigerant system is not suitable to set up in laboratory.

To model the position-dependent characteristics in the experimental system, the illustrated plot for the three-phase Y-connected 4-pole BDCM is shown in Fig. 2 where only equivalent windings a_1, a_1', a_2, a_2' of phase a and the magnetic poles of the rotor in the dashed circle are also plotted.

The mass of the copper cylinder is M and the stator winding a_1 is fixed at position θ_{r0}. Radius r is the distance between the center of the aluminum disk and the mounting position of the copper cylinder. When the rotor is rotating, all parts coupled to the shaft are also rotating. Therefore, the gravity force Mg of copper cylinder with fixed downward direction may either accelerate or decelerate the motor speed according to the rotor position θ_r. It follows that the copper cylinder would contribute to a position-dependent load torque $T_{L,pd}(\theta_r)$

$$T_{L,pd}(\theta_r) = Mgr\cos\theta_r \tag{1}$$

It is noted that the average value of the position-dependent load torque $T_{L,pd}(\theta_r)$ over one period is zero. In order to yield the position-dependent characteristics of refrigerant compressors, a constant load torque should be included into the experimental system. Therefore, in the M-G set, the Generator-end terminals are connected to the Y-connected resistors to provide a constant load torque $T_{L,dc}$ independent of the rotor position θ_r.

From the mechanical equation, the generating torque T_e, the load torque T_L and BDCM speed ω_r are related by

$$T_e - T_L = J\frac{d\omega_r}{dt} + B\omega_r \tag{2}$$

where B is the damping coefficient and J is the total inertias of the rotor, the coupled disk and the copper cylinder.

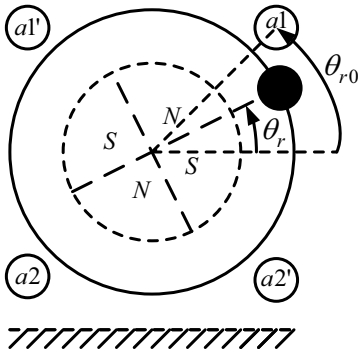

Fig. 2. Illustrated plot for position-dependent load torque.

The load torque T_L can be divided into a constant load torque $T_{L,dc}$ and an position-dependent ac component $T_{L,pd}$ with zero average value.

When a 4-pole BDCM coupled with a position-dependent load torque rotates at speed $\omega_r = d\theta_r/dt = \overline{\omega}_r + \Delta\omega_r$ with averaged speed $\overline{\omega}_r$, its generating torque T_e can also be divided into dc component $T_{e,dc}$ and a varying component $T_{e,ac}$ with zero average value. Then, (2) can be rewritten as

$$(T_{e,dc} + T_{e,ac}) - (T_{L,dc} + T_{L,pd}) = J\frac{d\omega_r}{dt} + B\omega_r \tag{3}$$

Moreover, in the steady state, all the terms $B\overline{\omega}_r$, the dc torque components $T_{e,dc}$ and $T_{L,dc}$ in (3) must be cancelled. Due to small damping coefficient B and small speed variation $\Delta\omega_r$, the damping term $B\Delta\omega_r$ can be neglected. Therefore, (3) can be simplified and rewritten as

$$T_{e,ac}(\theta_r) - T_{L,ac}(\theta_r) \approx J\frac{d^2\theta_r}{dt^2} \tag{4}$$

If we let the generated motor torque $T_{e,ac}$ vary with the same function $\cos(\theta_r)$ as the position-dependent load torque in (1), the expression in (4) can be simplified as

$$\Delta T\cos(\theta_r) \approx J\frac{d^2\theta_r}{dt^2} \tag{5}$$

where ΔT is the torque difference between $T_{e,ac}$ and $T_{L,pd}$. However, by integrating (5), the rotor position $\theta_r(t)$ in *rads* can be approximated as

$$\theta_r(t) \approx \overline{\omega}_r t - \frac{\Delta T}{J\overline{\omega}_r^{\,2}}[1 - \cos(\overline{\omega}_r t)] \tag{6}$$

$$\omega_r(t) \approx \overline{\omega}_r - \frac{\Delta T}{J\overline{\omega}_r}\sin(\overline{\omega}_r t) \tag{7}$$

Some waveforms for the illustrated case ($\theta_{r0} = \pi/12$) are plotted in Fig. 3 where e_U, e_V and e_W are the induced back-EMFs per phase. In order to possess efficient torque generating capability, BDCMs must draw winding currents i_U, i_V and i_W synchronized with their back-EMFs e_U, e_V and e_W, respectively.

In a 4-P BDCM, the electrical angular frequency in *rads*/*sec* is double mechanical angular frequency in *rads*/*sec*. Therefore, within each complete rotating cycle, there are two complete electrical cycles and twelve current commutations for a 4-pole BDCM. It follows that the commutation intervals are $\pi/6$ mechanical degrees (i.e. $\pi/3$ electrical degrees), and thus, each commutation instant t_k in square-current control must occur at the rotor position θ_r equal to

$$\theta_r(t_k) = 2\theta_{r0} + \frac{k\pi}{6},\ k \text{ is an integer} \tag{8}$$

From (8), it is noted that the difference of rotor position between consequent commutation position $\theta_r(t_k)$ and $\theta_r(t_{k-1})$ is fixed and equal to $\pi/6$. By using (6), the fixed position difference $\theta_r(t_k) - \theta_r(t_{k-1})$ of commutation can be expressed as

$$\begin{aligned}\theta_r(t_k) - \theta_r(t_{k-1}) &= \frac{\pi}{6}\\ &\approx \overline{\omega}_r\Delta t_k + \frac{\Delta T}{J\overline{\omega}_r^{\,2}}[\cos(\overline{\omega}_r t_k) - \cos(\overline{\omega}_r t_k - \overline{\omega}_r\Delta t_k)]\end{aligned} \tag{9}$$

where Δt_k ($= t_k - t_{k-1}$) denotes the commutation interval between each commutation instant. By applying the common

equality $\cos(A-B)=\cos A\cos B+\sin A\sin B$, (9) can be rewritten as

$$\frac{\pi}{6}\approx\overline{\omega}_r\Delta t_k+\frac{\Delta T}{J\overline{\omega}_r^2}A[\cos(\overline{\omega}_r t_k-\phi)] \tag{10}$$

where

$$A=\sqrt{[1-\cos(\overline{\omega}_r\Delta t_k)]^2+\sin(\overline{\omega}_r\Delta t_k)^2} \tag{11}$$

and

$$\phi=\tan^{-1}[\frac{\sin(\overline{\omega}_r\Delta t_k)}{1-\cos(\overline{\omega}_r\Delta t_k)}] \tag{12}$$

By considering the actual case, the product of $\overline{\omega}_r\Delta t_k$ would fluctuate around $\pi/6$ which leads to the following useful approximation

$$\cos(\overline{\omega}_r\Delta t_k)\approx\cos(\frac{\pi}{6})\approx 0.866 \tag{13}$$

By replacing (13) into (11) and (12), we can obtain $A\approx 0.52$ and $\phi\approx 5\pi/12$. Therefore, (10) can be rearranged as

$$\Delta t_k\approx\frac{\pi}{6\overline{\omega}_r}-\frac{0.52\Delta T}{J\overline{\omega}_r^3}[\cos(\overline{\omega}_r t_k-\frac{5\pi}{12})] \tag{14}$$

However, we can expand (14) to become a time-delay expression form as

$$\cos(\overline{\omega}_r t_{k-m})\approx\cos(\overline{\omega}_r t_k-\frac{m\pi}{6}) \tag{15}$$

where m must be an integer. Consequently, the commutation interval Δt_k in (14) can be rewritten as either

$$\Delta t_k\approx\frac{\pi}{6\overline{\omega}_r}-\frac{0.52\Delta T}{J\overline{\omega}_r^3}[\cos(\overline{\omega}_r t_{k-2})] \tag{16}$$

or

$$\Delta t_k\approx\frac{\pi}{6\overline{\omega}_r}-\frac{0.52\Delta T}{J\overline{\omega}_r^3}[\cos(\overline{\omega}_r t_{k-3})] \tag{17}$$

From (16) and (17), we can find that the current commutation interval Δt_k can be seen as a time-delay function of $\cos(\overline{\omega}_r t_k)$. On the other hand, it means that the position-dependent load torque $\Delta T\cos(\overline{\omega}_r t_k)$ can be observed either from the future commutation period Δt_{k+2} or from Δt_{k+3}.

$$\Delta T\cos(\overline{\omega}_r t_k)\approx\frac{\frac{\pi J\overline{\omega}_r^2}{6}-J\overline{\omega}_r^3\Delta t_{k+2}}{0.52} \tag{18}$$

or

$$\Delta T\cos(\overline{\omega}_r t_k)\approx\frac{\frac{\pi J\overline{\omega}_r^2}{6}-J\overline{\omega}_r^3\Delta t_{k+3}}{0.52} \tag{19}$$

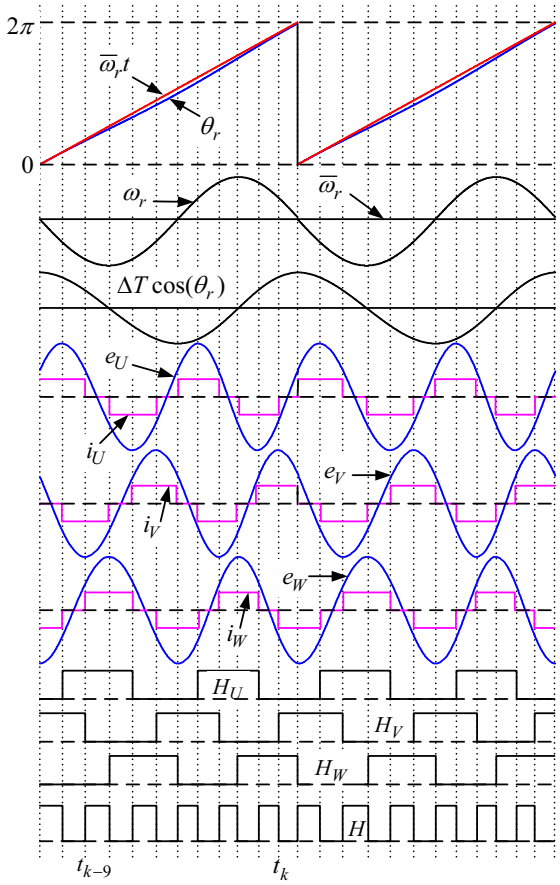

Fig. 3. Illustrated waveforms for a 4-P BDCMs.

However, estimation from future information is not practical. In steady state, the position-dependent torque is repetitive, and each commutation interval can be assumed to be equal to the previous twelfth commutation interval i.e. $\Delta t_k=\Delta t_{k-12p}$ where p is an integer. Therefore, in order to obtain practical implementation, (18) and (19) can be simplified to obtain the following practical equations

$$\Delta T\cos(\overline{\omega}_r t_k)\propto\frac{\pi}{6}-\overline{\omega}_r\Delta t_{k-9} \tag{20}$$

$$\Delta T\cos(\overline{\omega}_r t_k)\propto\frac{\pi}{6}-\overline{\omega}_r\Delta t_{k-10} \tag{21}$$

where the current load torque difference $\Delta T\cos(\overline{\omega}_r t_k)$ is proportional to the deviation of the product $\overline{\omega}_r\Delta t_{k-9}$ or $\overline{\omega}_r\Delta t_{k-10}$ from $\pi/6$.

III. Position Sensorless Control

The system configuration of the proposed robust sensorless control is plotted in Fig. 4. The main difference between the conventional sensorless control and the proposed robust sensorless control is that the control signal v_{cont} is yielded by the product of the output of the speed control and the adaptive gain G_k [4]. That is, the conventional sensorless control can be seen as the special case of the robust sensorless control plotted in Fig.5 with fixed unity gain $G_k=1$.

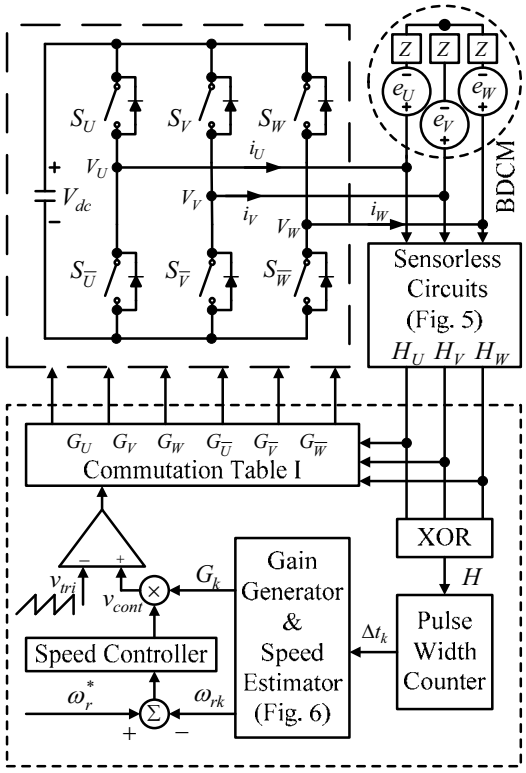

Fig. 4. System configuration of the proposed robust sensorless controller.

A. Sensorless Starting Strategy

The starting strategy used in the sensorless control can be divided into three modes: agitation mode, alignment mode and synchronization mode. Before the motor rotating in agitation mode, the sleeping refrigerant is initially agitated to be flowing easily, and then, the rotor is forced to locate in a given position in alignment mode with commutation state F shown in Table I. In synchronizing mode, the six commutation signals $G_U \sim G_{\overline{W}}$ start generating and changing with the series A => B => C => D => E => F => A… to draw winding currents to compose a synchronous rotating magnetic field with increasing speed. Once the rotor reaches to some speed at which the sensorless circuits are able to function well, the speed loop turn to work to generate the six commutation signals according to the sensorless commutation table in Table I.

Table I: Sensorless commutation table

States	$(H_U\ H_V\ H_W)$	S_U	$S_{\overline{W}}$	S_V	$S_{\overline{U}}$	S_W	$S_{\overline{V}}$
A	(0 1 1)	OFF	ON	PWM	OFF	OFF	OFF
B	(0 1 0)	PWM	ON	OFF	OFF	OFF	OFF
C	(1 1 0)	PWM	OFF	OFF	OFF	OFF	ON
D	(1 0 0)	OFF	OFF	OFF	OFF	PWM	ON
E	(1 0 1)	OFF	OFF	OFF	ON	PWM	OFF
F	(0 0 1)	OFF	OFF	PWM	ON	OFF	OFF

B. Sensorless Circuit

The alternative rotor position signals H_U, H_V and H_W are generated from sensing the terminal voltages V_U, V_V and V_W through the sensorless circuit as shown in Fig. 5. In order to commutate currents without any position sensor, the used sensorless circuit can be divided into three stages: 90° phase shifting stage, dc filtering stage and PWM filtering stage. The first stage obtains alternative position signals from 90° shifting the sensed floating terminal voltage by the low-pass filter. The latter two stages are designed to attenuate the undesired low-frequency and PWM components from the sensed terminal voltages [4].

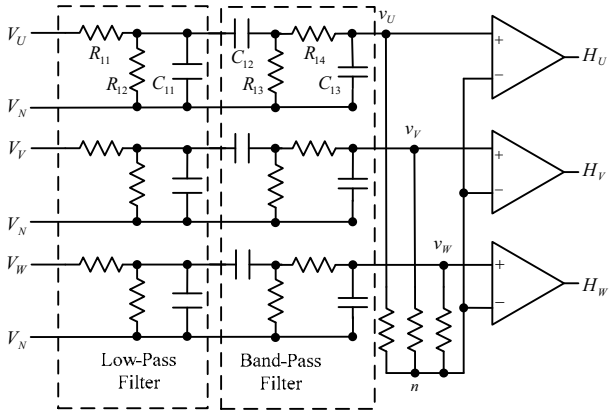

Fig. 5. Sensorless circuits.

C. Sensorless Speed Estimation

Unlike the conventional speed loop where the controller output directly controls the output voltage, an varying gain G_k is included to change the control signal v_{cont} according to the position-dependent load torque. After using the exclusive-or (XOR) operator, the three position signals are combined to single position signal H. Then, each commutation period Δt_k can be directly obtained from counting the duration between each rising/falling edge of position signal H. For 4-pole BDCMs, the average speed ω_{rk} in *rpm* can be calculated from the commutation period Δt_k by

$$\omega_{rk} = \frac{60}{\sum_{n=0}^{11} \Delta t_{k-n}} \tag{22}$$

D. Robust Speed Control

Based on (20), the profile of the position-dependent load torque $\Delta T(\theta_r)$ can be estimated from the commutation period Δt_k. It implies that by generating adequate gain G_k, we can vary the PWM duty ratio and thus, change the winding currents and motor torque in order to oppose to the position-dependent load torque. For simplicity, the adaptive gain G_k can be obtained by

$$G_k = 1 + \sum_{m=0}^{k} \left[W\left(\frac{\Delta t_{m-9}}{\sum_{n=0}^{11} \Delta t_{m-n}} - \frac{1}{12} \right) \right] \tag{23}$$

where the weighting factor W is used to adjust the gain sensitivity to Δt_k. It is noted that no motor parameters can be fond in (23). It follows that the proposed robust sensorless control possesses good parameter insensibility.

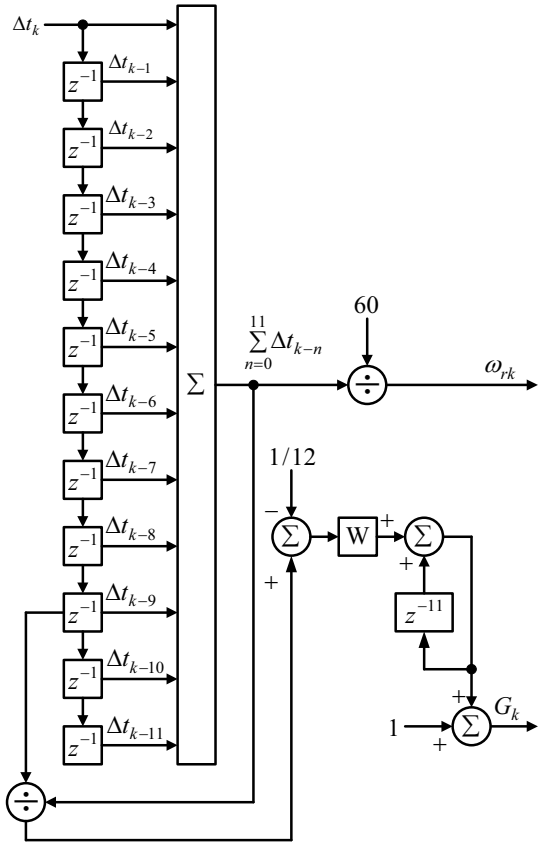

Fig. 6. Gain generator and speed estimation.

IV. Simulation Results

From (19) and Fig. 5, we can find that the proposed sensorless control with fixed unity gain $G_k = 1$ is analogous to the conventional speed control for BDCM. The simulated waveforms are plotted in Fig. 7 where the proportional-integral (PI) type is used in the speed controller. Some nominal values and circuit elements are listed in Table II.

Table II: Simulated parameters

Stator resistance	0.7Ω
Stator inductance	$Lq = 10.5mH$, $Ld = 4mH$
Voltage constant (Line-to-Line)	$23.63\ mV_{rms} / rpm$
Pole number	4 pole
Motor inertia	$0.0004\ Kg - m^2$
DC link voltage	$300\ V$
PWM frequency	$5kHz$
Average load torque	$1\ Nm$

From Fig. 7(a), we can find that the actual speed ω_r deviates from the speed command ω_r^* due to the repetitive position-dependent load torque in Fig. 7(b). We also can find that the load torque is position-dependent function $T_L = 1 + 0.5\cos\theta_r$ (N-m) from Fig. 7(b) and Fig. 7(c). Owing to the position-dependent load torque, speed estimation delay at high speed is smaller than that at low speed, the speed ripples are about $120rpm$ and $100rpm$ at $\omega_r^* = 1200rpm$ and $\omega_r^* = 1500rpm$, respectively. In Fig. 7(d), it is noted that the control signal v_{cont} fluctuates according to the speed error between the speed command ω_r^* and the speed estimation ω_{rk}. In addition, the control signal v_{cont} is almost at its valley and peak when the load torque is near its maximum and minimum values, respectively. It means that the control signal v_{cont} adjusts by itself to resist the position-dependent load torque. However, such adversity would aggravate the speed ripple. Therefore, we propose the robust sensorless control to alleviate the speed ripple due to the position-dependent load torque.

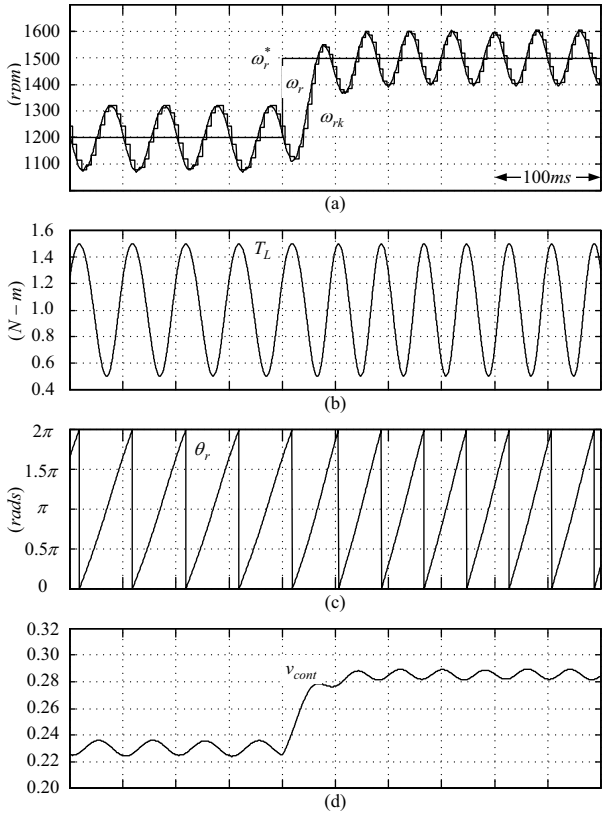

Fig. 7. Simulated waveforms with fixed unity gain $G_k = 1$ due to the change of speed command ω_r^* from 1200rpm to 1500rpm: (a) actual speed ω_r and the estimated speed ω_{rk}; (b) position-dependent load torque T_L; (c) rotor position θ_r and (d) control signal v_{cont}.

To evaluate the proposed robust sensorless control, some simulated results with the same controller parameter as Fig. 8 are illustrated in Fig. 8 where varying gain G_k is included. Compared with the speed ripple in Fig. 7(a), the speed variation in Fig. 8(a) is reduced to about near zero with the same speed controller parameter and the same speed estimation delay. It demonstrates that the developed algorithms in (16) through (20) make the sensorless operation possess robust speed performance to the position-dependent load torque.

From Fig. 8(b) and Fig. 8(d), the gain G_k reflects the useful estimation of the load torque T_L which can help the speed controller to reverse the adversity in Fig. 8(b) and Fig. 8(d). That is, by complying with the system stability, we can adequately set the weighing factor W in (23) as large as possible to adjust the final control signal v_{cont} in phase with the load torque variations. From Fig. 8(e), we can find that the control signal v_{cont} fluctuates effectively to generate motor torque to position-dependent load torque.

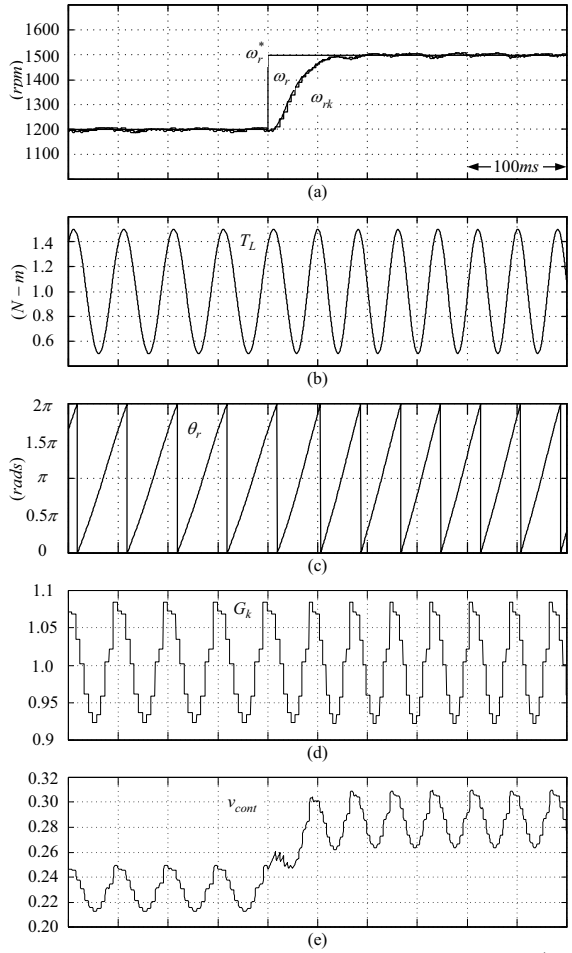

Fig. 8. Simulated waveforms due to the change of speed command ω_r^* from 1200*rpm* to 1500*rpm*: (a) actual speed ω_r and the estimated speed ω_{rk} ; (b) position-dependent load torque T_L ; (c) rotor position θ_r ; (d) duty gain G_k ; and (e) control signal v_{cont} .

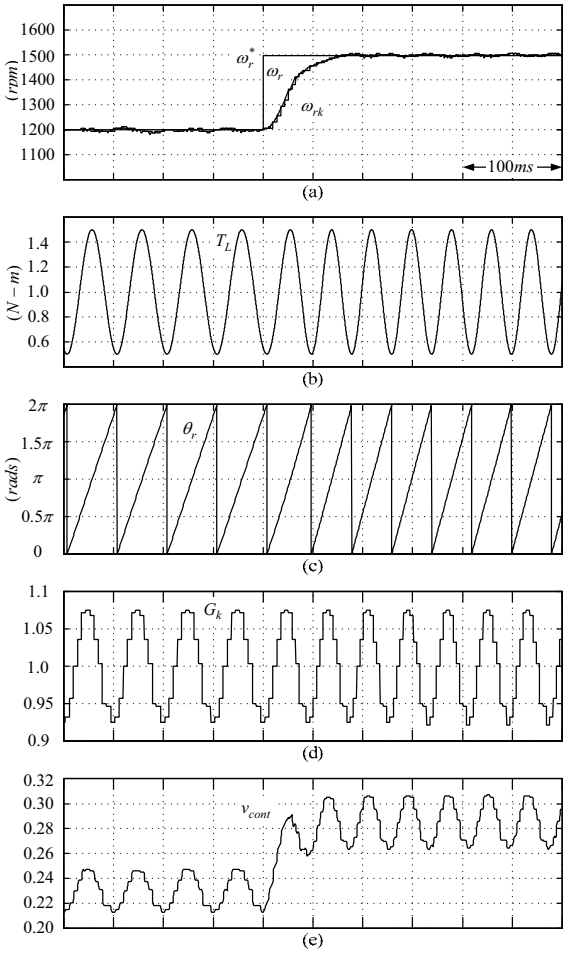

Fig. 9. Simulated waveforms due to the change of speed command ω_r^* from 1200*rpm* to 1500*rpm*: (a) actual speed ω_r and the estimated speed ω_{rk} ; (b) position-dependent load torque T_L ; (c) rotor position θ_r ; (d) duty gain G_k ; and (e) control signal v_{cont} .

To show the robustness of developed sensorless controller to load torque of various absolute positions, the simulated waveforms for the case of $T_L = 1 - 0.5\cos\theta_r$ (N-m) are plotted in Fig. 9. Obviously, the duty gain G_k is also almost at its valley and peak values when the load torque is near its maximum and minimum values, respectively. It follows that near zero speed ripple can be found in Fig. 9(a).

V. CONCLUSIONS

Without any position sensors, the motor terminal voltages were sensed to generate the helpful position signals to correctly commutate winding currents. A mathematical model of repetitive position-dependent load torque was developed in this paper. The model was then used to obtain the algorithms of the proposed position sensorless control where the PWM duty was not only dependent on the speed controller output but also on the yielded duty gain. The provided simulated results had demonstrated the proposed sensorless control.

REFERENCES

[1] H. Murakami, Y. Honda, H. Kiriyama, S. Morimoto, and Y. Takeda, "The Performance Ccomparison of SPMSM, IPMSM and SynRM in Use as Air-Conditioning Compressor," in *Proc. IAS'99*, pp. 840-845, 1999.

[2] S. Ogasawara, and H. Akagi, "An Approach to Position Sensorless Drive for Brushless DC Motors," *IEEE Trans. Ind. Applicat.,* vol.27, no. 5, pp. 928-933, 1991.

[3] H. C. Chen, and C. M. Liaw, **"**Current-Mode Control for Sensorless BDCM Drive with Intelligent Commutation Tuning," *IEEE Trans. Power Electron.,* vol. 17, no. 5, pp. 747-756, 2002.

[4] H. C. Chen, Y. C. Chang, and C. K. Huang, 'Practical Sensorless Control for Inverter-Fed BDCM Compressors,' *IET Proc. Electric Power Applications,* vol. 1, no. 1, pp. 127-132, Jan. 2007.

[5] E. Delaleau and A. M. Stankovic, "Modeling and Simulation of the Induction Motor with Position-Dependent Load Torque," in *Proceedings of the 42nd Conference on Decision and Control*, pp. 6212-6217, 2003.

[6] P. Krishnamurthy, W. Lu, and A. Keyhani, "A Robust Force Controller for an SRM Based Electromechanical Brake System," in *Proceedings of the 44th Conference on Decision and Control*, pp. 2006-2011, 2005.

[7] Z. Kovacic, S. Bogdan and M. Balenovic, "A Model Reference & Model-based Self-learning Fuzzy Logic Controller as a Solution for Control of Nonlinear Servo System*," IEEE Trans. Energy Conversion*, vol. 14, no. 5, pp. 1479-1484, Dec. 1999.

[8] J. Solsona and M. I. Valla, and C. Muravchik, "Nonlinear Control of a Permanent Magnet Synchronous Motor with Disturbance Torque Estimation*," IEEE Trans. Energy Conversion*, vol. 15, no. 2, pp. 163-168, Jun. 2000.